Structural Study of Amorphous Co-Ferrite Film by Anomalous X-Ray Scattering

E. Matsubara, K. Okuda, and Y. Waseda

Research Institute of Mineral Dressing & Metallurgy (SENKEN), Tohoku University, Sendai, 980 Japan

S. N. Okuno and K. Inomata

Research and Development Center, Toshiba Corporation, Komukai Toshiba-cho, Saiwai-ku, Kawasaki, 210 Japan

Z. Naturforsch. **45a**, 1144–1150 (1990); received June 16, 1990

The structure of amorphous Co-ferrite film grown on a glass substrate was studied by anomalous X-ray scattering (AXS). Co atoms cannot be distinguished from Fe atoms with the usual X-ray diffraction technique. Therefore the AXS method at the Fe and Co K-absorption edges was adopted. In the previous AXS studies only the lower energy side of the absorption edges was adopted. In the previous AXS studies only the lower energy side of the absorption edge was used. In the present case, the lower energy side of the Co K-absorption edge corresponds to the higher energy side of the Fe K-absorption edge. Therefore, in order to overcome this inconvenience, the scattering was measured on both sides of the absorption edge, thus enabling the independent determination of the oxygen coordination numbers around Co and Fe in the ferrite film from the environmental RDFs estimated from the energy differential profiles by coupling with the linear least squares technique.

Introduction

The X-ray atomic scattering factor is described by $f(Q, E) = f^0(Q) + f'(E) + if''(E)$. The value of f^0 corresponds to the normal atomic scattering factor in usual X-ray scattering experiments with the radiation of an energy away from any absorption edge. The quantities of f' and f'', which are the real and imaginary parts of the anomalous dispersion terms, are usually almost constant in a wide energy range and show an abrupt change only near the absorption edge. The variation of f' and f'' causes a change of scattering intensities. Thus, when the energy of the incident X-rays is tuned to the close vicinity of the absorption edge of a certain constituent element A and this energy region differs sufficiently from those of the absorption edge of other elements in a sample, the intensity variation stemms only from a change of the X-ray scattering factor of the element A. Therefore, the local chemical environment can be determined by analyzing the energy dependence of the intensity. This technique of Anomalous X-ray Scattering (AXS) is based upon the idea of Hosoya [1] and Shevchik [2] and was first used by Fuoss et al. [3] with synchrotron radiation under the name of differential anomalous scattering (DAS). In our previous AXS measurements, a large drop of f' at the lower energy side of the K- or L_{III}-absorption edge was used, because at the higher energy side of the edge extremely intense fluorescence radiates from the sample and the values of f' theoretically calculated do not give a good agreement with the experimental values in terms of the so-called EXAFS (Extended X-ray Absorption Fine Structure) and XANES (X-ray Absorption Near Edge Structure) signals just above the absorption edge. Successful results have been obtained using this AXS method with respect to the structure of several oxide glasses, such as GeO_2 [4], $ZnO_2P_2O_5$ [5], $La_{1-x}Sr_xMnO_3 \cdot B_2O_3$ [6], Bi_2O_3–CaO–Fe_2O_3 [7], and so on.

The amorphous $CoFe_2O_{4-x}$ film prepared by ion beam sputter deposition has recently been found to show the spin glass behavior [8]. The near-neighbor atomic correlations of Fe and Co or the local chemical environments around Fe and Co are strongly required to understand this interesting magnetic property. However, Fe and Co are the next neighbors in the periodic table and the lower energy side of the Co K-absorption edge just corresponds to the higher energy side of the Fe K-absorption edge. Therefore,

Reprint requests to Dr. E. Matsubara, Research Institute of Mineral Dressing and Metallurgy, Tohoku University, Sendai 980, Japan.

0932-0784 / 90 / 0900-1144 $ 01.30/0. – Please order a reprint rather than making your own copy.

the assumption made in the AXS method explained above is not true anymore. Thus, the conventional AXS method must be modified to overcome some problems resulting from the use of both sides of the absorption edges, and new general equations for the AXS analysis should also be derived.

The main purpose of this work is to present the fundamentals of this modified AXS method for separately determining the local environment of neighboring elements in the periodic table and its application to amorphous Co ferrite film grown on a glass substrate.

Principle of the Modified AXS Method

In the present AXS analysis, both the real and imaginary part of the anomalous dispersion varies with the incident energy since both sides of the absorption edge of a certain selected element A are used. Furthermore, variations of the anomalous dispersion terms of the other elements may not be small in the energy region around the absorption edge of A. Thus, the contribution from all the constituent elements to the intensity difference must be taken into account. Consequently, the difference between the scattering intensities measured at two energies E_1 and E_2 is given by

$$\Delta i(Q, E_1, E_2) = I(Q, E_1) - I(Q, E_2) = \sum_{j=1}^{n} \sum_{k=1}^{n} c_j F_{jk}(Q, E_1, E_2) \cdot \int_0^{\infty} 4\pi r^2 (\varrho_{jk}(r) - \varrho_{0k}) \frac{\sin(Qr)}{Qr} \mathrm{d}r, \quad (1)$$

$$I(Q, E_1) = I_{\mathrm{eu}}^{\mathrm{coh}}(Q, E_1) - \sum_{j=1}^{n} c_j f_j^*(Q, E_1) f_j(Q, E_1), \quad (2)$$

$$F_{jk}(Q, E_1, E_2) = \mathrm{Re}[f_j(Q, E_1)]\,\mathrm{Re}[f_k(Q, E_1)] + f_j''(E_1) f_k''(E_1) - \mathrm{Re}[f_j(Q, E_2)]\,\mathrm{Re}[f_k(Q, E_2)] - f_j''(E_2) f_k''(E_2). \quad (3)$$

The term of c_j is the atomic fraction of an element j, n the number of constituent elements, $\varrho_{jk}(r)$ the number density function of an element k around an element j, and ϱ_{0j} the average number density for an element j. Re is the real part of the value in the parentheses.

The environmental radial distribution function (RDF) is determined by the Fourier transformation of the quantity $Q\Delta i(Q, E_1, E_2)$:

$$4\pi r^2 \sum_{j=1}^{n} \sum_{k=1}^{n} \frac{c_j F_{jk}(Q, E_1, E_2)}{W(Q, E_1, E_2)} \varrho_{jk}(r) = 4\pi r^2 \varrho_0 + \frac{2r}{\pi} \int_0^{\infty} \frac{Q\Delta i(Q, E_1, E_2)}{W(Q, E_1, E_2)} \sin(Qr)\,\mathrm{d}Q, \quad (4)$$

$$W(Q, E_1, E_2) = \sum_{j=1}^{n} \sum_{k=1}^{n} c_j c_k F_{jk}(Q, E_1, E_2). \quad (5)$$

ϱ_0 is the average number density.

Experimental

An amorphous film was prepared by ion-beam sputtering of a target made of a sintered body of polycrystalline $CoFe_2O_4$. The sputtering were carried out with a beam of argon ions accelerated to 1 keV in an oxygen-gas flow of 0.5×10^{-4} Torr. More details of the sample preparation have been given in [8]. The film of 865 nm thickness was grown on a glass substrate.

The scattering intensity from the amorphous film (I_{samp}) was measured with the Seemann-Bohlin geometry. The angle of incidence α was 0.75° and 1.0° in the AXS measurements and 1.2° in the measurement with Mo Kα. The contribution of the substrate was taken account of by multiplying the absorption correction for the amorphous film (A_{film}) with the intensity from the substrate (I_{sub}) measured under exactly the same experimental conditions, and subtracting the product from I_{samp}:

$$I_{\mathrm{film}} = I_{\mathrm{samp}} - A_{\mathrm{film}} I_{\mathrm{sub}}, \quad (6)$$

$$A_{\mathrm{film}} = \exp\left\{-2\mu_f t_f \frac{\sin\theta\cos(\theta-\alpha)}{\sin\alpha\sin(2\theta-\alpha)}\right\}, \quad (7)$$

where μ_f and t_f are the linear absorption coefficient and thickness of the film, respectively.

The AXS scattering was measured with synchrotron radiation at the Photon Factory of the National Laboratory for High Energy Physics, Tsukuba, Japan. Monochromatic incident beams were obtained with a double Si 111 crystal monochromator whose optimum energy resolution is about 7 eV at 10 keV. The intensity of the incident beam was monitored with an ion chamber placed in front of the sample. The measured intensities were converted to intensities in

counts per photon by dividing by the total number of photons calculated from the monitor counts [7]. Diffracted intensities were measured by a portable pure germanium solid-state detector in order to separately collect the coherent intensity and the fluorescent radiations from the sample. The incident energies used for the present AXS measurements were 6.811, 7.086, 7.534, 7.684 and 8.309 keV, which are 300 and 25 eV below the Fe K-absorption edge (7.111 keV), 175 and 25 eV below the Co K-absorption edge (7.706 keV) and 600 eV above the Co K-absorption edge, respectively. Since the effect of the higher harmonics diffracted by the Si (333) plane was significant in these measurements, the intensity of the higher harmonics was reduced to less than 0.5% by intentionally detuning the second Si crystal of the double crystal monochromator with a piezo electric device attached to it. Incidentally, the intensity of the first order diffraction was reduced to 80% in this operation. At least 20 000 counts were collected at every scattering angle, and more than 45 000 counts were collected at the first peak of each incident energy. Although the incident energy of 7.086 keV is below the Fe K-absorption edge, Fe fluorescence was observed, mainly arising from the tail of the band pass. Fe Kβ fluorescence overlapping with the coherent radiation was estimated from the intensity of Fe Kα radiation and the ratio of Fe Kα to Fe Kβ [9], and subtracted from the coherent scattering [10]. Similarly, in the measurement at 7.684 keV, Co Kβ fluorescence overlaps with the coherent scattering. Since Fe fluorescence was also observed and Co Kα fluorescence was collected with Fe Kβ fluorescence, the intensities of Fe Kα fluorescence, the mixture of Fe Kβ and Co Kα fluorescence and the Co Kβ fluorescence overlapping with the coherent intensity were separately collected. Using these measured intensities with the ratios of Kα to Kβ for Fe and Co, the intensity of Fe Kβ, then that of Co Kα and finally that of Co Kβ were estimated. This Co Kβ was subtracted to obtain the coherent intensity alone. More details of the experimental setting and data processing have been described in [11]. For a comparison, the ordinary RDF which describes the average structure of the sample was also determined, using the monochromatic Mo Kα radiation obtained by a Ge 111 single crystal monochromator in incident beams. The scattering intensity was measured with a scintillation counter with a pulse-height analyzer.

In the measurement below the Fe K-absorption edge, the intensity from the substrate corrected for the absorption by the film is about 20% of the total scattering intensity from the sample. However, in the measurement above the Fe K-absorption edge, this contribution is less than 4% because the absorption coefficient of the film above the edge is larger than 4 times the absorption coefficient below the edge. This becomes more prominent in the measurement above the Co K-absorption edge, where the contribution from the substrate is almost negligible. On the other hand, in the measurement with Mo Kα, about 80 to 90% of the total intensity is ascribed to the intensity from the substrate. These scattering intensities from the amorphous film were corrected for the polarization and absorption, and converted to absolute units by the generalized Krogh-Moe-Norman method [12] with the X-ray atomic sattering factors tabulated in [13] and anomalous dispersion terms computed [14] by Cromer and Liberman's method [15], followed by the correction of the Compton scattering intensity with the Breit-Dirac factors [16].

From the resultant coherent intensity $I_{eu}^{coh}(Q)$ for the Mo Kα-radiation, the ordinary interference function $Qi(Q)$ was calculated by

$$Qi(Q) = \{I_{eu}^{coh}(Q) - \langle f^2 \rangle + \langle f \rangle^2\} / \langle f \rangle^2, \quad (8)$$

where $\langle f \rangle$ is the average atomic scattering factor and $\langle f^2 \rangle$ is the mean square of the atomic scattering factor. The ordinary RDF was obtained by the Fourier transform of $Qi(Q)$:

$$4\pi r^2 \varrho(r) = 4\pi r^2 \varrho_0 + \frac{2r}{\pi} \int_0^\infty Qi(Q) \sin(Qr)\, dQ, \quad (9)$$

where $\varrho(r)$ is the average radial density function.

Results and Discussion

The corrected coherent scattering intensity profile in electron units per atom ($I_{eu}^{coh}(Q)$) for the amorphous $CoFe_2O_{4-x}$ film measured with Mo Kα is shown in Figure 1. The profile indicates a non-crystalline structure. The interference function $Qi(Q)$ computed from $I_{eu}^{coh}(Q)$ by (8) is shown in Figure 2. The fundamental feature of $Qi(Q)$ is similar to those of some silicate and phosphate glasses [17]. Namely, the profile is composed of the first peak at 24 nm^{-1}, followed by several quite distinct oscillations, which contrasts to amorphous alloys in which oscillations in $Qi(Q)$ are rapidly damped to zero. If species having definite bond lengths and angles exist, persistence of the oscil-

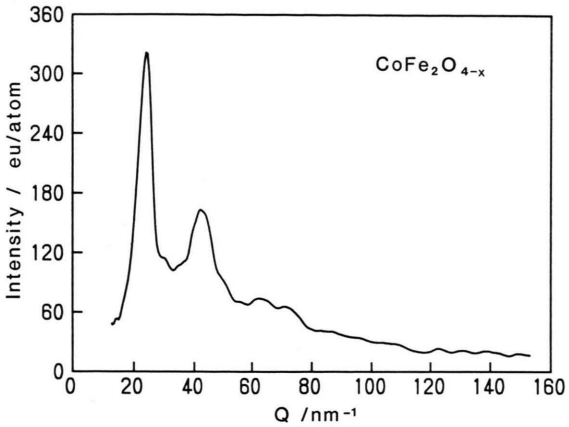

Fig. 1. Scattering intensity profile from amorphous $CoFe_2O_{4-x}$ film with Mo Kα-radiation.

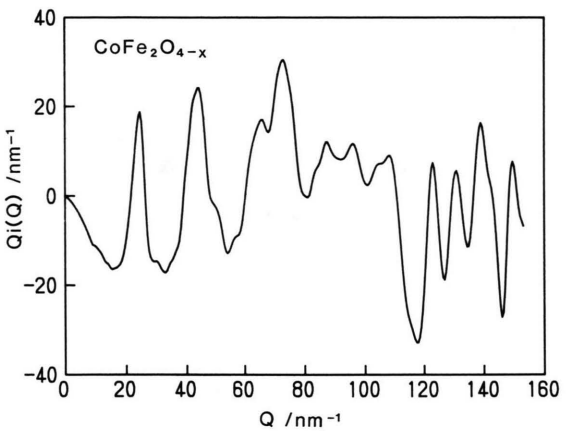

Fig. 2. Interference function $Qi(Q)$ of amorphous $CoFe_2O_{4-x}$ film with MoKα-radiation.

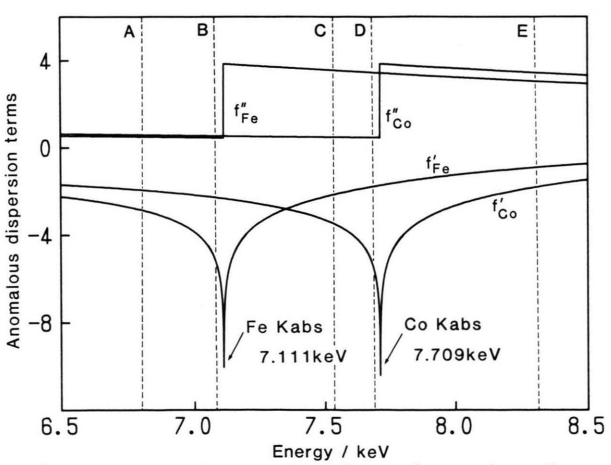

Fig. 3. Theoretical energy dependence of anomalous dispersion terms for Fe and Co near the K-absorption edge, as calculated by Cromer and Liberman's method.

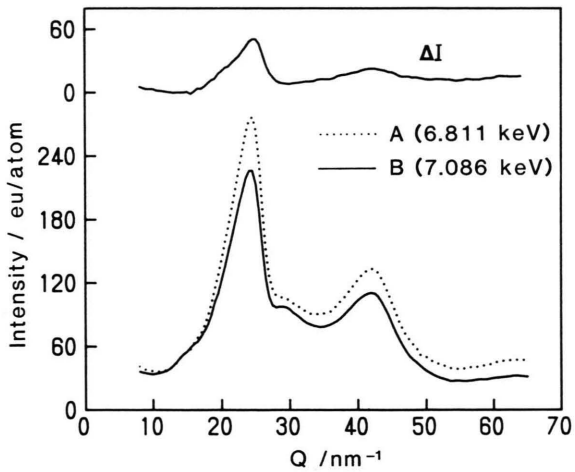

Fig. 4. Differential intensity profile of amorphous $CoFe_2O_{4-x}$ film (top) obtained from the intensity profiles (bottom) measured at incident energies of 6.811 and 7.086 keV, which correspond to energies of 25 and 300 eV below the Fe K-absorption edge.

lations in $Qi(Q)$ would be clearly detected even in the high-Q region [18, 19]. Thus, the oscillations observed in this oxide glass clearly imply that a considerable fraction of the transition metals form a quite rigid local ordering structure although the distribution of these local units appears to be completely random.

Theoretical values of the real and imaginary parts of the anomalous dispersion terms for Fe and Co, as computed [14] with Cromer and Liberman's method [15], are plotted in Fig. 3 vs. energy. The incident energies used in the present AXS measurements are indicated with vertical broken lines labeled A to E in Figure 3. In order to obtain the energy differential profile, three kinds of combinations of the intensity profiles at the two energies of A and B, C and D, and D and E were selected. The AXS measurement at A and B was treated in a similar manner as in our conventional AXS method [4], where variations of the real part of the anomalous dispersion terms are only utilized at the lower energy side of the edge of Fe. The intensity profiles observed at A and B, and the energy differential profile (ΔI) defined as their difference are shown in Figure 4. Using the area and position of the first peak in the environmental RDF around Fe estimated from ΔI by the conventional AXS method, it is found that Fe atoms are surrounded by 4.7 ± 0.3 oxygens with the average distance of 0.202 nm. However, it should be noted that this analysis is not exactly correct in the present case because the real parts of Co

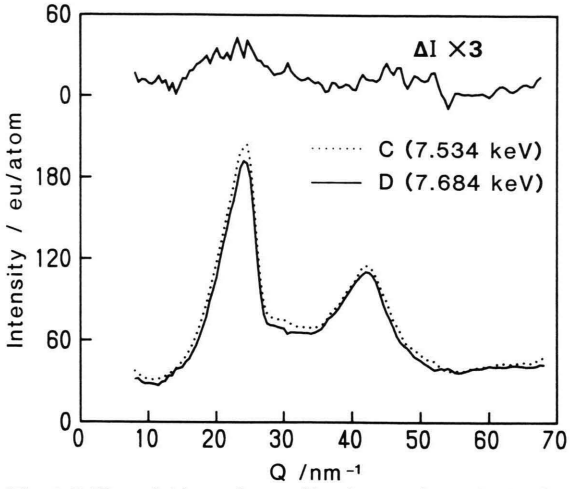

Fig. 5. Differential intensity profile of amorphous $CoFe_2O_{4-x}$ film (top) obtained from the intensity profiles (bottom) measured at incident energies of 7.534 and 7.684 keV, which correspond to energies of 25 and 175 eV below the Co K-absorption edge.

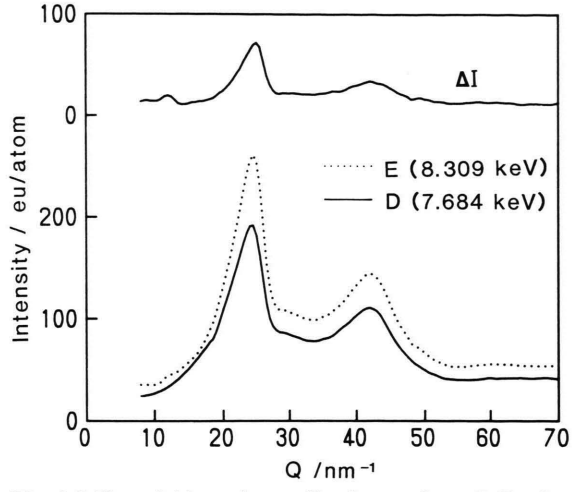

Fig. 6. Differential intensity profile of amorphous $CoFe_2O_{4-x}$ film (top) obtained from the intensity profiles (bottom) measured at incident energies of 7.684 and 8.309 keV, which correspond to energies of 25 eV below and 600 eV above the Co K-absorption edge.

(f'_{Co}) and Fe(f'_{Fe}) change at the two energies of A and B. In other words, the environmental RDF obtained with the conventional method in the present case represents not only the environmental structure around Fe but also that around Co. The amount of variation of f'_{Co} is about 13% of those of f'_{Fe} between A and B. Thus, in the environmental RDF obtained from the energy differential profile at A and B, the contribution from the Co–O pairs, for example, is about 7% of that from the Fe–O pairs. Furthermore, this contribution fraction is proporional to the ratio of the atomic concentrations of Co and Fe. In the present case, the atomic concentration of Fe is twice that of Co. This means that the smaller the fraction of Fe relative to Co, the larger becomes the contribution of Co–O pairs.

Two important problems are brought up in the measurement between the two neighboring absorption edges. The AXS measurement takes place at the two energies of C and D in Fig. 3 in the present study. The first problem is that the contributions from Fe as well as from Co are included. The variations of f'_{Fe} at C and D are about 18% of those of f'_{Co}. Furthermore, since the sign of the variation with energy is positive for f'_{Fe} and negative for f'_{Co}, the intensity difference caused by the change of f'_{Co} at C and D is reduced due to the change of f'_{Fe}. The second problem is that because of the presence of the EXAFS signal of Fe on the higher energy side of the Fe K-absorption edge, the difference between the two incident energies selected for the AXS measurement is not large enough to obtain a large variation in f'_{Co}. In the present case, the energies C and D are about 420 and 570 eV above the Fe K-absorption edge. Referring to the EXAFS spectrum of Fe [20], the error caused by the EXAFS signal was estimated to be $<2\%$ at C and $<0.5\%$ at D. In terms of these two unfavorable restrictions in the AXS measurement, the differential intensity profile is rather reduced, as it is clearly seen in Figure 5. Then, the AXS measurement with two energies between next neighboring absorption edges may not be a good choice.

The combination of the intensity profiles at the two energies of D and E in Fig. 3 was also used. The important feature of this AXS measurement is that the large variations of f'_{Co} as well as f''_{Co} are utilized. Thus, the intensity difference at D and E becomes much larger than that a C and D, which is readily seen in the differential profile of Figure 6. In this combination, another important feature is notified. Namely, although the differential profile also represents the environmental structure around Fe as well as Co, the contribution from the atomic configurations around Fe to the differential intensity is much smaller than that in the AXS measurement at C and D. It is readily understood in Fig. 3 that the variation of f'_{Fe} between D and E is much smaller than that between C and D.

The ordinary RDF obtained by the Fourier transformation of the interference function $Qi(Q)$ in Fig. 2

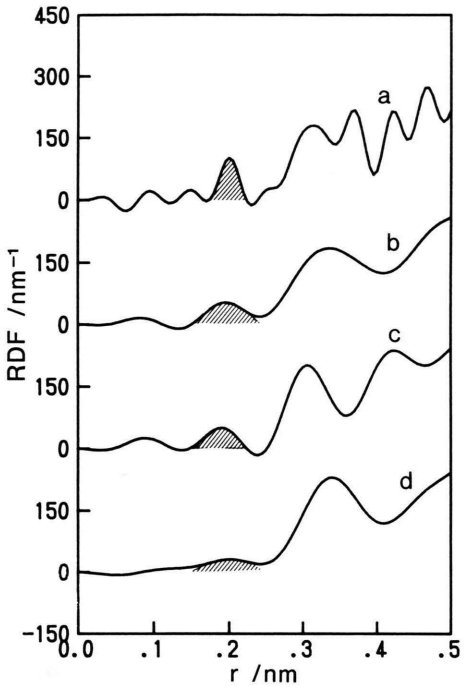

Fig. 7. Ordinary radial distribution function (RDF) (curve a) and environmental RDFs determined from the differential intensity profiles in Fig. 4 (curve b), Fig. 5 (curve c) and Fig. 6 (curve d) (density = 4.69 Mg/m^3).

is shown as curve (a) in Fig. 7 with the environmental RDFs (curves (b) to (d)) computed from the nergy differential profiles in Figs. 4 to 5. Referring to the atomic distances between nearest-neighboring oxygen and transition metals in the spinel $CoFe_2O_4$ structure (0.182 and 0.207 nm), the hatched peaks in Fig. 7 are ascribed to the Co–O and Fe–O pairs. As discussed above, these environmental RDFs include the structural information both around Fe and Co although the contribution from each element is varied in every measurement. In other words, the present environmental RDF data represent the partial structural factors of Fe–O, Co–O and Fe–Co pairs except that of the O–O pair. Consequently, the coordination numbers of oxygen atoms around Fe and Co can be determined from the area under the hatched peaks in Figure 7. The area under the peak in the environmental RDF is not directly related to the coordination number for a j–k pair, $N_{jk} = 4\pi r^2 \varrho_{jk}(r)$. As defined in (4) and (5), the value of N_{jk} is computed by dividing the area by the coefficient of N_{jk}, that is, $w_{jk} = c_j F_{jk}(Q, E_1, E_2)/W(Q, E_1, E_2)$. This coefficient depends on the anomalous dispersion terms of j and k. The coefficients of Co–O and Fe–O pairs computed for each environmental RDF are tabulated in Table 1. Similarly, the coefficient of the coordination number in the ordinary RDF is defined by $c_j f_j(Q, E_1) f_k(Q, E_2)/\langle f \rangle^2$. It is clearly seen that there is a relation between the coordination numbers for Co–O and Fe–O pairs and the areas under peaks, that is, (area) $= w_{FeO} N_{FeO} + w_{CoO} N_{CoO}$. Four independent equations exist for the two unknowns N_{FeO} and N_{CoO}. Thus, by applying the simple linear least squares technique to these equations, it is found that Fe and Co atoms are surrounded by 5.2 ± 0.6 and 6.3 ± 0.4 oxygens, respectively. Taking account of the experimental errors, the value of N_{FeO} obtained above from the AXS measurement at the lower energy side of the Fe K-absorption edge, gives a good agreement with the value by the linear least squares technique. The detailed discussion about the structure of amorphous $CoFe_2O_{4-x}$ film is outside the scope of this work. Nevertheless, the following possible interpretation for the local ordering units may be suggested. Both FeO_4 tetrahedra and FeO_6 octahedra exist as the fundamental local ordering units around Fe and CoO_6 octahedra are the fundamental units around Co.

Table 1. Coefficients for Fe–O and Co–O pairs and areas under the first peaks in the RDFs.

Incident energy (keV)		Coefficients		Area
		Fe–O	Co–O	
17.447		0.400	0.209	2.73
6.811,	7.086	0.492	0.033	2.79
7.534,	7.684	−0.274	0.773	3.29
8.309,	7.684	0.138	0.307	2.82

I conclusion, obviously next neighboring elements in the periodic table cannot be distinguished with X-ray diffraction. However, by cleverly using the AXS method one can deduce more than the average structure even in a system including next neighboring elements in the periodic table, as it has been demonstrated using the result of the amorphous Co-ferrite film, as an example.

We (E.M. and Y.W.) particularly want to thank the staff of Photon Factory, National Laboratory for High Energy Physics, Drs. M. Nomura and A. Koyama.

[1] S. Hosoya, Bull. Phys. Soc. Japan **25,** 110 (1970).
[2] N. J. Shevchik, Phil. Mag. **35,** 805 (1977).
[3] P. H. Fuoss, P. Eisenberger, W. K. Warburton, and A. Bienenstock, Phys. Rev. Lett. **46,** 1537 (1981).
[4] E. Matsubara, K. Harada, Y. Waseda, and M. Iwase, Z. Naturforsch. **43a,** 181 (1988).
[5] E. Matsubara, K. Sugiyama, Y. Waseda, M. Ashizuka, and E. Ishida, J. Mater. Sci. Lett. **9,** 14 (1990).
[6] E. Matsubara, Y. Waseda, K. Inomata, and S. Hashimoto, Z. Naturforsch. **44a,** 723 (1989).
[7] E. Matsubara, Y. Waseda, M. Mitera, and T. Masumoto, Trans, Japan Inst. Met. **29,** 697 (1988).
[8] S. N. Okuno, S. Hashimoto, K. Inomata, S. Morimoto, and A. Ito, J. Mag. Soc. Japan **14,** 213 (1990).
[9] N. V. Rao, S. B. Reddy, G. Satyanarayana, and D. L. Sastry, Physica **138c,** 215 (1986).
[10] S. Aur, D. Kofalt, Y. Waseda, T. Egami, R. Wang, H. S. Chen, and B. K. Teo, Solid State Commun. **48,** 111 (1983).
[11] Y. Waseda, E. Matsubara, and K. Sugiyama, Sci. Rep. Res. Inst. Tohoku Univ. A **34,** 1 (1988).
[12] C. N. J. Wagner, H. Ocken, and M. L. Joshi, Z. Naturforsch. **20a,** 325 (1965).
[13] International Tables for X-ray Crystallography, vol. IV, The Kynoch Press, Birmingham 1974, p. 99.
[14] Y. Waseda, Novel Application of Anomalous X-ray Scattering for Structural Characterization of Disordered Materials, Springer-Verlag, New York 1984, p. 119.
[15] D. T. Cromer and D. Liberman, J. Chem. Phys. **53,** 1891 (1970).
[16] D. T. Cromer, J. Chem. Phys. **50,** 4857 (1969).
[17] E. Matsubara, T. Kawazoe, Y. Waseda, M. Ashizuka, and E. Ishida, J. Mat. Sci. **23,** 547 (1988).
[18] Y. Waseda, Structure of Non-Crystalline Materials, McGraw-Hill, New York 1980, p. 133.
[19] K. Suzuki and P. A. Egelstaff, Can. J. Phys. **52,** 241 (1974).
[20] M. Nomura, KEK Internal 87-1 (1987), p. 53.